Kinetic instability of AlGaN alloys during MBE growth under metal-rich conditions on m-plane GaN miscut towards the -c axis

M. Shirazi-HD, R. E. Diaz, T. Nguyen, J. Jian, G. C. Gardner, H. Wang, M. J. Manfra, and O. Malis

Citation: Journal of Applied Physics **123**, 161581 (2018);
View online: https://doi.org/10.1063/1.5011413
View Table of Contents: http://aip.scitation.org/toc/jap/123/16
Published by the American Institute of Physics

Kinetic instability of AlGaN alloys during MBE growth under metal-rich conditions on m-plane GaN miscut towards the -c axis

M. Shirazi-HD,[1,2] R. E. Diaz,[2] T. Nguyen,[3] J. Jian,[4] G. C. Gardner,[2,4] H. Wang,[4] M. J. Manfra,[1,2,3,4] and O. Malis[3,a)]
[1]*School of Electrical and Computer Engineering, Purdue University, West Lafayette, Indiana 47907, USA*
[2]*Birck Nanotechnology Center, West Lafayette, Indiana 47907, USA*
[3]*Department of Physics and Astronomy, Purdue University, West Lafayette, Indiana 47907, USA*
[4]*School of Materials Engineering, Purdue University, West Lafayette, Indiana 47907, USA*

(Received 31 October 2017; accepted 11 January 2018; published online 31 January 2018)

$Al_xGa_{1-x}N$ layers with Al-composition above 0.6 ($0.6 < x < 0.9$) grown under metal-rich conditions by plasma-assisted molecular beam epitaxy on m-plane GaN miscut towards the -c axis are kinetically unstable. Even under excess Ga flux, the effective growth rate of AlGaN is drastically reduced, likely due to suppression of Ga-N dimer incorporation. The defect structure generated during these growth conditions is studied with energy dispersive x-ray spectroscopy scanning transmission electron microscopy as a function of Al flux. The AlGaN growth results in the formation of thin Al(Ga)N layers with Al-composition higher than expected and lower Al-composition AlGaN islands. The AlGaN islands have a flat top and are elongated along the c-axis (i.e., stripe-like shape). Possible mechanisms for the observed experimental results are discussed. Our data are consistent with a model in which Al-N dimers promote release of Ga-N dimers from the m-plane surface. *Published by AIP Publishing*. https://doi.org/10.1063/1.5011413

INTRODUCTION

Nonpolar m-plane AlGaN/GaN heterostructures are interesting from both a fundamental material growth perspective and for practical applications in infrared optoelectronic devices.[1–12] Intersubband optoelectronic devices utilize optical transitions within the conduction band of GaN/AlGaN quantum wells to emit or detect infrared radiation. The accessible wavelength range is mainly determined by the conduction band-offset between the well and the barrier material, i.e., GaN and AlGaN in this case. High Al-composition AlGaN is needed to access the technologically important telecommunications range (1.55 μm). Moreover, infrared nonpolar nitride devices theoretically benefit from the absence of built-in polarization fields that allows better control of the transition energy and enhanced optical transition strength. To date, promising experimental results have been reported for near- and far-infrared intersubband absorption and photodetection in m-plane nitride heterostructures utilizing limited Al-composition alloys.[2–12] Mid-infrared intersubband absorption in m-plane AlGaN/GaN heterostructures grown by metal-organic chemical vapor deposition (MOCVD) was demonstrated by Kotani *et al.*[4–6] We reported far-infrared (THz) intersubband absorption in AlGaN/GaN superlattices grown by molecular beam epitaxy (MBE).[2] Lim *et al.*[7–11] also demonstrated short- to long-wavelength infrared intersubband transitions in MBE-grown AlGaN/GaN heterostructures. Nevertheless, to fully realize the potential of m-plane nitrides for infrared devices, high aluminum composition AlGaN is needed. This paper focuses on the growth of m-plane AlGaN/GaN superlattices by plasma-enhanced MBE under metal-rich conditions and the defect structure generated during this process.

The growth phase diagram of nonpolar m-plane AlGaN/GaN heterostructures is not completely established,[13–19] unlike the corresponding process for similar c-plane structures. Evident differences arise from the anisotropy of adatom mobilities along the c- and a-axis on the m-plane surface during growth,[20,21] and the anisotropic lattice mismatch between GaN and AlN along the c-direction (4%) and the a-direction (2.5%). Equally importantly, however, the m-plane surface and its primary step edges (c-type and a-type) present atomic composition and dangling bond geometries that are markedly different from those available for growth on the c-plane surface. The compounded effect of all these parameters in the range of high Al-composition has not been sufficiently investigated to date either theoretically or experimentally.

Sawicka *et al.* examined the growth of $Al_xGa_{1-x}N$ ($x \leq 0.1$) by MBE under N-rich conditions, and identified formation of AlN precipitates.[13–16] We have successfully grown uniform m-plane AlGaN/GaN superlattices with Al-composition up to $Al_{0.2}Ga_{0.8}N$,[2,3,17,18] but encountered challenges when increasing Al-composition above 20%. Lim *et al.* also investigated the effect of Al-incorporation on the infrared optical properties of AlGaN/GaN m-plane multi-quantum wells, but no results were reported for Al composition between 45% and 99%.[7–11] Reports of Kotani *et al.* are also limited to alloys below 50% Al composition, and did not contain any in depth structural analysis of the samples used in mid-infrared intersubband absorption measurements.[4–6] This paper concentrates on the defect structure of high Al-composition m-plane $Al_xGa_{1-x}N$/GaN ($x > 0.5$) superlattices. We chose to perform the growth under metal-rich conditions because these conditions have been shown to be optimal for c-plane AlGaN

a)Author to whom correspondence should be addressed: omalis@purdue.edu

growth.[1,19] We found that $Al_xGa_{1-x}N$ MBE growth is unstable under Ga-rich conditions in the $x = 0.6$–0.9 Al-composition range on m-plane GaN, and is characterized by a distinctly different growth mode that has not been observed in nitride materials on other crystal orientations, or in other material systems. This growth mode can be referred to as Al-limited growth in the presence of excess Ga. It leads to the formation of specific nanostructures consisting of lower Al-content flat-top islands oriented mainly parallel to the c-axis on top of higher Al-content thin, continuous films. Several mechanisms that may be responsible for the observed behavior are discussed. Our data support a model that involves Al-N dimers promoting dissociation of Ga-N dimers. The Ga-N dimers released from the lattice float on the surface and desorb, or are incorporated into GaN layers after all Al flux is consumed.

EXPERIMENTAL

The m-plane AlGaN/GaN heterostructures were grown by plasma-assisted MBE on commercially available free-standing m-plane GaN substrates provided by Nanowin. The GaN substrates are either semi-insulating or n-type, and have a typical root-mean-square (rms) roughness of 0.2–0.3 nm over 16 μm^2 and a threading dislocation density of $<5 \times 10^6\,cm^{-2}$. The nominal miscut of the substrates is 1° towards the -c axis (no miscut towards the a-axis). The rectangular substrates (5 mm $\times$ 10 mm) were mounted with liquid Ga on larger c-plane GaN-on-sapphire wafers. Gallium and aluminum fluxes were supplied by conventional effusion cells and nitrogen flux was provided by a Veeco Unibulb radio-frequency plasma source operating at 300 W forward power with 0.5 sccm of nitrogen (N_2) flow. The substrate temperature was measured with a pyrometer to be 720 °C. The N-limited growth rate of m-plane GaN is 8.8 nm/min under these conditions, and it is the same, within experimental error, as on c-plane GaN.

All samples were grown under constant Ga-rich conditions with Ga/N $\sim$ 1.55 and Al-fluxes as specified. The atomic fluxes were calibrated using growth rates established by high-resolution x-ray diffraction (HRXRD), and the monolayer atom density of 1.21×10^{15} atoms/cm.[2] The Al fluxes were scaled linearly from the growth rate measured by HRXRD for a 15-period $Al_{0.03}Ga_{0.97}N$/GaN superlattice (fixed Al beam-flux 1.93×10^{13} atoms/cm^2/s), assuming that the $Al_{0.03}Ga_{0.97}N$ and GaN growth rates are the same.

Two types of AlGaN/GaN structures were grown for this investigation: structures with varying Al flux or AlGaN thicknesses for scanning transmission electron microscopy (STEM) only, and 15-period superlattices with fixed aluminum flux and layer thicknesses for high-resolution x-ray diffraction (HRXRD) measurements. We note that HRXRD of the samples with varying parameters cannot be easily interpreted, but STEM of the superlattices with fixed parameters provides information in agreement with the data discussed below. The samples with varying Al flux or AlGaN thicknesses were grown to simultaneously image in STEM multiple different growth conditions while varying only one parameter, either Al-flux or growth time. This is difficult to achieve in many consecutive sample growths due to run-to-run variability of the MBE parameters. Furthermore, analysis of the impact of a change in growth parameters within a single sample designed for STEM analysis is more straightforward. Table I shows the summary of the growth parameters for samples A and B discussed in detail below. Sample A was grown to examine the dependence of the AlGaN structure on Al flux and to identify the transition to the instability regime. Sample A consists of five 3-period AlGaN/GaN superlattices (A1-A5) grown with increasing Al-flux. The growth time for each layer is the same (60 s), with an additional 3 min growth pause (all shutters closed) between superlattices to change the Al flux. Sample B was grown to study the time evolution of the AlGaN structure in the instability regime. Sample B consists of five 3-period superlattices (B1-B5) with increasing AlGaN growth times (15, 30, 45, 60, and 75 s) and constant Al flux of 1.63×10^{14} atoms/cm^2/s.

Samples for STEM imaging and analysis were prepared using the focused ion beam (FIB) lift-out technique with a FEI Nova 200 DualBeam, and later thinned to transparency in a Nanomill at 900 eV. The STEM images were taken on a FEI Talos 200 kV with a Super X EDS detector.

The 15-period superlattices with fixed growth conditions were characterized by HRXRD. The HRXRD data were collected using a PANalytical X'Pert-MRD high-resolution x-ray diffractometer equipped with a four-bounce Ge monochromator and analyzed using the commercial software package PANalytical X'PERT EPITAXY. Satellite peaks were observed confirming the existence of superlattice structures. The HRXRD spectra were fitted to extract information

TABLE I. Summary of growth parameters for the two samples examined with STEM-EDX shown in Fig. 1 (sample A) and Fig. 3 (sample B). Each sample consists of five 3-period superlattices grown in the order A1-A5 and B1-B5, respectively.

Sample	Superlattice (3-period)	GaN growth time (s)	AlGaN growth time (s)	Al flux atoms/cm^2/s	Ga flux atoms/cm^2/s	N flux atoms/cm^2/s
Sample A	A1	60	60	9.07×10^{13}	1.0×10^{15}	6.43×10^{14}
	A2	60	60	1.13×10^{14}	1.0×10^{15}	6.43×10^{14}
	A3	60	60	1.44×10^{14}	1.0×10^{15}	6.43×10^{14}
	A4	60	60	1.63×10^{14}	1.0×10^{15}	6.43×10^{14}
	A5	60	60	1.89×10^{14}	1.0×10^{15}	6.43×10^{14}
Sample B	B1	60	15	1.63×10^{14}	1.0×10^{15}	6.43×10^{14}
	B2	60	30	1.63×10^{14}	1.0×10^{15}	6.43×10^{14}
	B3	60	45	1.63×10^{14}	1.0×10^{15}	6.43×10^{14}
	B4	60	60	1.63×10^{14}	1.0×10^{15}	6.43×10^{14}
	B5	60	75	1.63×10^{14}	1.0×10^{15}	6.43×10^{14}

about the nanostructure, but only the superlattice period is an independent parameter. In order to estimate the AlGaN layer thickness and Al-composition, we typically assume that the GaN growth rate is constant as measured on the c-plane. Cross-sectional STEM substantiates this claim. More accurate determination of the layer thicknesses and Al-composition is possible if STEM and HRXRD data are combined for the same sample.

RESULTS

Our focus is on the effect of aluminum flux on the structure of high Al-composition m-plane AlGaN grown by MBE under metal-rich conditions. Figure 1 illustrates the effect of increasing Al-flux on the growth of the AlGaN layers in sample A under constant Ga flux. We found that the average superlattice period (i.e., thickness of AlGaN/GaN pair) drops rapidly with increasing Al beam flux even though excess Ga is provided at all times. This drop is mainly due to the decrease in the growth rate and structural changes of the AlGaN layers. STEM evidence suggests that the pure GaN growth rate is less affected, but it may be slightly increased right after AlGaN growth. Most notably, the third (top) GaN layer of each superlattice has a thickness larger than the first two GaN layers due to additional GaN growth from excess surface Ga after all shutters are closed. This excess Ga is due in part to the high Ga flux provided at all times during the growth, but also to Ga released from the lattice by Al, as discussed below.

At low Al fluxes (superlattices A1 and A2), the AlGaN layers maintain a relatively smooth surface. However, even at the lowest Al-flux (9.07×10^{13} atoms/cm^2/s) that results in $Al_{0.2}Ga_{0.8}N$ deposition (established with HRXRD on a uniform, fixed Al-flux superlattice sample), the AlGaN growth rate (7.9 nm/min) is 10% lower than the GaN growth rate (8.8 nm/min) for the same provided Ga flux. A relatively small increase in Al flux from 9.07×10^{13} atoms/cm^2/s to 1.13×10^{14} atoms/cm^2/s produces $Al_{0.24}Ga_{0.76}N$ layers that exhibit intercalated planar defects made of high Al-fraction AlGaN [Fig. 1(b)]. Further increasing the Al-flux leads simultaneously to a drop of the superlattice period and super-linear increase of the effective Al-composition of the barriers. For the superlattice grown with 1.44×10^{14} atoms/cm^2/s Al-flux, an average Al composition above 50% and average AlGaN growth rate of 2.5 nm/min can be determined from HRXRD of a different, fixed Al flux sample. We emphasize that in this case the concepts of the average growth rate and average Al-composition as established with HRXRD must be applied with caution, since such values are strongly dependent on the assumptions made for the HRXRD fit. Yet, this AlGaN growth rate is considerably lower than the growth rate of 8.8 nm/min expected for the provided III/N ratio in a typical metal-rich (N-limited) growth.

For Al-fluxes higher than 1.44×10^{14} atoms/cm^2/s, AlGaN growth produces a unique nanostructure of thin film plus flat-top anisotropic islands aligned mostly along the c-axis visible in superlattices A4-A5 in Fig. 1(a). The Al flux that corresponds to the transition from smooth to nanostructured films is hard to determine exactly and depends on a variety of growth parameters including the film thickness and surface morphology due to miscut. Nevertheless, under the growth conditions used here, $Al_xGa_{1-x}N$ with $x > 0.6$ clearly transforms into nanostructured films. A close examination of the nanostructure grown with Al fluxes above 1.44×10^{14} atoms/cm^2/s indicates that the AlGaN layers are also non-uniform in composition. Essentially, homogeneous growth of m-plane $Al_xGa_{1-x}N$ with an Al composition between approximately 0.6 and 0.9 is unstable under conditions corresponding to metal-rich plasma-enhanced MBE.

The flat-top islands grown with Al-fluxes higher than 1.44×10^{14} atoms/cm^2/s appear to be anisotropic, stripe-like, predominantly elongated in the c-direction at least for the lower end of the flux range. The islands become taller and sharper with increasing Al flux. Well-defined m-type nanofacets [$(10\bar{1}0)$ and $(0\bar{1}10)$] bordering the stripes are visible in the view along the c-axis in Fig. 1(a). In the view along the a-axis, distinct islands become evident only at the highest Al flux [Fig. 1(b)].

Figure 2 shows the energy dispersive x-ray spectroscopy (EDX) elemental maps of Ga and Al in the superlattice A5 grown using an Al flux of 1.89×10^{14} atoms/cm^2/s. EDX elemental maps and Z-contrast STEM images show in both cases the compositional inhomogeneity of the AlGaN barriers. Figure 2(d) shows Ga and Al linear composition change across the AlGaN/GaN superlattice grown with the

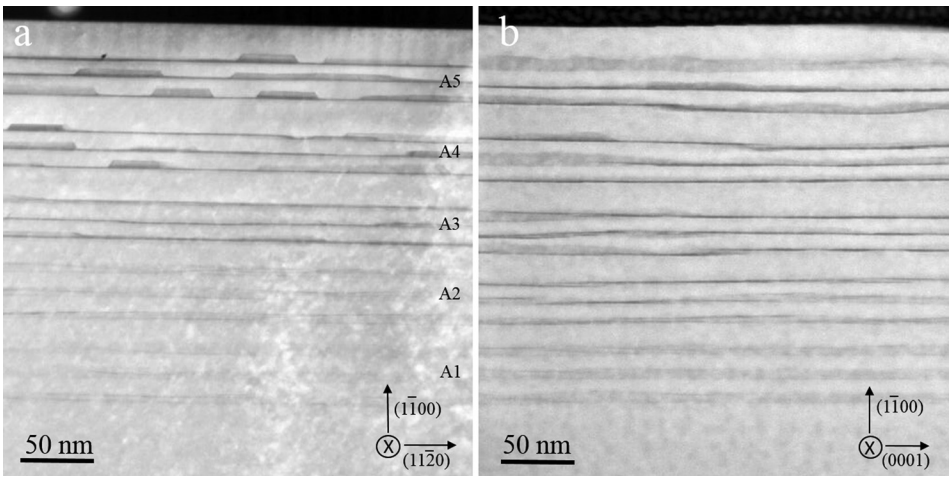

FIG. 1. High-angle annular dark field (HAADF) STEM images of sample A that consists of five 3-period AlGaN/GaN superlattices (A1-A5) grown with increasing Al beam flux. Images were taken along the c-axis (a) and along the a-axis (b). GaN is bright and AlGaN is dark in the images. The growth direction is up. The 5 superlattices were separated by a 3 min growth pause that resulted in an increase of the top GaN layer thickness due to excess Ga incorporation.

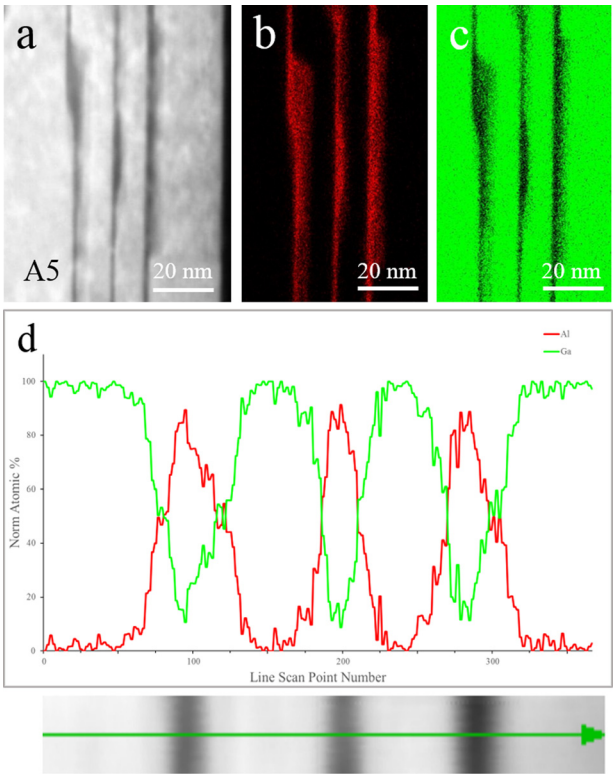

FIG. 2. HAADF STEM image (a), and corresponding Al (b) and Ga (c) EDX elemental maps of superlattice A5 grown with the highest Al beam flux of 1.89×10^{14} atoms/cm^2/s and imaged along the c-direction [top in Fig. 1(a)]. (d) EDX-STEM elemental line scans for Ga and Al through the AlGaN/GaN superlattice A5 grown with the highest Al beam flux of 1.89×10^{14} atoms/cm^2/s. The growth direction is left to right.

highest Al flux of 1.89×10^{14} atoms/cm^2/s in a cross-section taken along the c-axis section. From the Z-contrast STEM image, we can clearly identify two regions: the bottom of the barrier (i), and the island on top of the barrier (ii). EDX quantitative analysis shows area (i) contains Al composition $x > 0.85$, while area (ii) has average Al composition of $x \approx 0.5$.

To examine the time dependence of the growth process in the instability regime, we have also grown a sample consisting of a sequence of five 3-period superlattices (sample B) with increasing AlGaN growth times (15, 30, 45, 60, and 75 s) and constant Al flux of 1.63×10^{14} atoms/cm^2/s (Fig. 3). For the shortest growth time (15 s), the AlGaN layers in B1 are fairly smooth, and have an approx. thickness of 1.4 nm, and Al composition of approx. 0.2 (established with EDX). When the AlGaN growth time increases, the film thickness does not increase proportionately, but the Al content increases rapidly, as if Al is replacing the already incorporated Ga. For 30 s of AlGaN growth in B2, the AlGaN layer thickness is also approx. 1.4 nm, within our experimental error, instead of the expected thickness of 2.8 nm (twice that for 15 s growth), and the Al composition increased to approx. 0.40. For longer growth times, the maximum Al composition reaches 0.8 and the flat-top stripe morphology described earlier nucleates and grows.

DISCUSSION

AlGaN growth by plasma-enhanced MBE on c-plane GaN has been studied extensively.[19] It was found that Al has a sticking coefficient equal to unity at all temperatures investigated, while Ga incorporation decreases with increasing Al-flux correlating with the remaining available active nitrogen after all Al is incorporated. When plasma conditions are kept constant, the c-plane AlGaN growth rate increases linearly with total metal flux and saturates at a maximum value given by the available active nitrogen flux. Segregation of Ga adatoms in the metal-rich regime was proposed by Iliopoulos *et al.* to explain c-plane AlGaN growth under high III-V ratio conditions.[22,23] They suggested that, under excess metal conditions, Ga adatoms are only weakly bonded to the surface (physi-sorption), and segregate into a surface metal layer that is prone to desorption. Meanwhile, the Al atoms are stronger bonded to the surface and fully incorporate into the c-plane growth. As a result, Ga acts as a surfactant and is incorporated only to the extent to which there are N atoms left available after the complete incorporation of Al.

We observe a substantially different process occurring during growth of AlGaN on m-plane GaN. Unlike c-plane

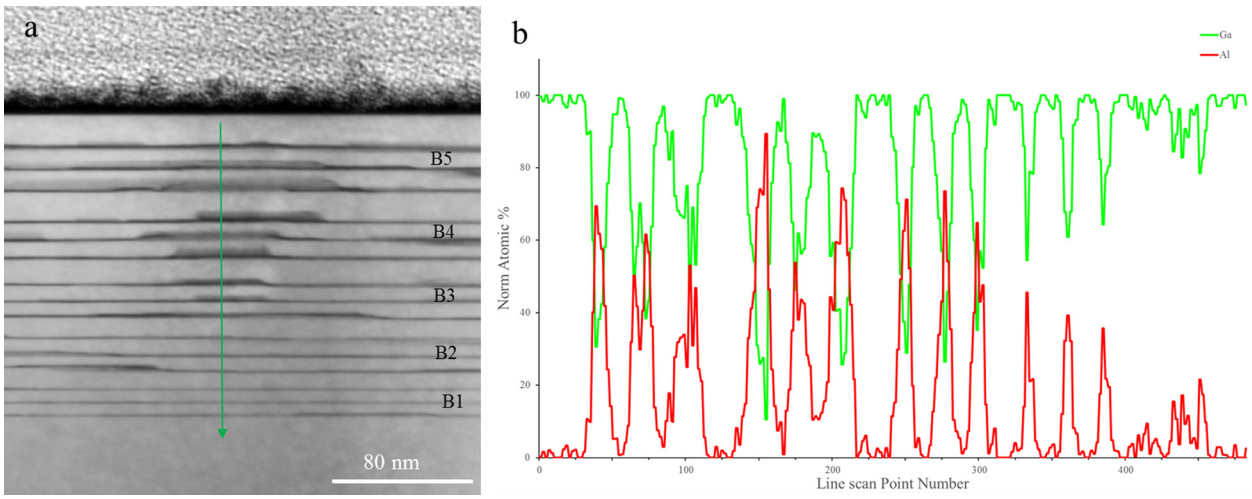

FIG. 3. STEM (a) and EDX elemental line scans (b) of sample B containing five 3-period AlGaN/GaN superlattices (B1-B5), all grown with an Al beam flux of 1.63×10^{14} atoms/cm^2/s but with increasing AlGaN growth time (bottom to top 15, 30, 45, 60, and 75 s). Note that the AlGaN layer (dark) thicknesses do not scale linearly with the growth time. The green arrow in (a) indicates the direction of the scan in (b). The growth direction in (b) is right to left.

growth, the m-plane AlGaN growth under excess Ga conditions is suppressed to such an extent that it cannot be explained by enhanced Ga desorption alone. In spite of large Ga adatom excess, and active N-flux sufficient to support a growth rate of 8.8 nm/min, Ga and N both appear to be prevented from incorporating into the alloy lattice in the presence of significant Al surface coverage. Therefore, this AlGaN growth mode may be referred to as Al-limited growth in the Ga-rich regime.

Sawicka *et al.*[14] examined growth of m-plane $Al_{0.1}Ga_{0.9}N$/GaN multi-quantum wells under nitrogen rich conditions by plasma-assisted MBE. They found the AlGaN to be rough and nonuniform in composition and attributed their observations to two main mechanisms: enhanced Ga desorption from the m-plane surface as compared to the c-plane surface, and instability of the m-plane surface to atomic nitrogen (i.e., N adatoms react with surface N atoms forming stable N_2 that desorbs[20]). However, their proposed mechanisms do not explain the abrupt drop of the alloy growth rate with Al-flux we observed under metal-rich conditions. Sawicka *et al.* also did not report on the growth of high Al-composition AlGaN. Horita *et al.* examined Ga incorporation into high Al-composition $(1\bar{1}00)$ and $(11\bar{2}0)$ AlGaN on 4H-SiC and found that almost no Ga is incorporated into $(11\bar{2}0)$ AlGaN, and that Ga is relatively little incorporated into $(1\bar{1}00)$ $Al_{1-x}Ga_xN$ $(x < 0.2)$.[24]

Our experimental results on m-plane AlGaN growth may be explained by surface phase segregation of Al adatoms near step edges and Ga adatoms away from the step edges. Ga may be blocked from reaching dangling bonds on the growth front (step-edges in step-flow growth mode) by an Al adatom layer that extends with increasing Al surface coverage [Fig. 4(a)]. Theoretical and experimental studies confirmed the stability of a Ga adatom layer on m-plane GaN, like the Ga adlayer on the c-plane surface.[25] Relatively little, though, is known about the structure of an Al adlayer, and the nanoscale phase diagram of the Ga-Al system on the m-plane GaN surface (the two metals are fully miscible in bulk at the growth temperature). At first impression, our Ga-rich conditions for AlGaN growth appear conducive to a continuous Ga adlayer on the surface. Moreover, the Al surface coverage is relatively low at any moment (Al/N ratio < 1) compared to the Ga coverage (Ga/N ratio > 1), so it is unlikely that an Al adlayer fully covers the surface. However, if Al adatoms segregate to the active step edges, they may provide sufficient coverage to effectively prevent Ga from reaching the edge and essentially only AlN can be grown. To confirm this model, more theoretical work is needed on the nanoscale phase diagram of Ga-Al alloys.

The above coarse-grain model explains some, but not all, of our experimental observations on m-plane AlGaN growth. Therefore, we propose an alternative atomistic mechanism for the growth instability of high Al-composition m-plane AlGaN. Our model builds on the results of Liu *et al.*[26] for first-principle calculations of step-flow homoepitaxial growth of m-plane GaN. Liu *et al.* emphasized that the energetics of atomic row nucleation and kink propagation at different types of step-edges are more important for predicting m-plane growth than single adatom surface mobility.[26] They also found that Ga-N dimers are more stable than isolated Ga and N adatoms, and the main feeding species for m-plane GaN growth.[26] Therefore, for AlGaN growth, we conclude that Al-N dimers should also be more stable than isolated Al and N atoms, and more stable than Ga-N dimers. Our proposed mechanism, shown schematically in Fig. 4(b), assumes that Al-N dimers destabilize GaN edges and release Ga-N dimers from edges. If Al is incorporated into the lattice without significantly affecting already attached Ga, the growth would proceed in the N-limited regime, analogous to c-plane growth, at a rate of 8.8 nm/min. The dramatic decrease of the net growth rate suggests that Al releases Ga from the lattice, most likely as Ga-N dimers. Consequently, our model involves interaction between Al-N and Ga-N dimers. We speculate that attachment of Al-N promotes detachment of Ga-N dimers that float on the surface and desorb in the presence of Al flux. Once the Al flux is terminated and all Al is consumed, the remaining Ga-N dimers on the surface are incorporated into the subsequent GaN layer. The larger than expected top GaN layer thickness mentioned earlier is evidence for this incorporation of excess Ga-N dimers after all sources are shuttered (growth pause).

Sequential attachment of Al-N dimers is energetically favored because Al-N dimers prefer to attach near other Al-N bonds triggering formation of planar AlN defects visible in Fig. 1(b). This process must be necessarily happening at the c-type edges (edges parallel to the a-axis), as they have the highest density on our -c-miscut GaN surfaces in the early stages of AlGaN growth. Moreover, the c-axis is the direction of maximum lattice mismatch between GaN and AlN, and therefore, strain may also play a major role in this process. A different process is proposed below to explain the behavior at the a-type edges (edges parallel to the c-axis) in the later stages of growth.

Composition inhomogeneities in AlGaN have been found under certain growth conditions by MOCVD on

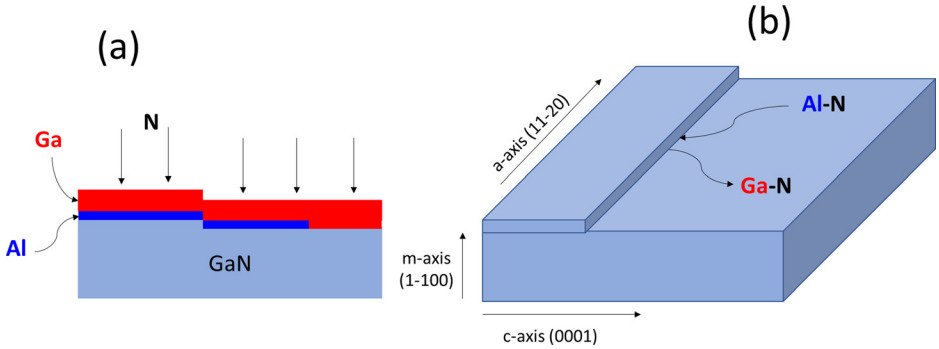

FIG. 4. Schematic representations of alternative mechanisms proposed to explain Al-limited AlGaN growth in Ga-rich MBE on m-plane GaN. (a) Al adatom segregation at step edges blocks Ga adatoms from reaching the growth front. (b) Al-N dimers promote detachment of Ga-N dimers mainly at c-edges leading to Al-rich alloys. The Ga-N dimers released from the lattice desorb or are incorporated into the top GaN layer during the growth pause (after all Al is consumed).

c-plane AlN and have been associated with surface morphology such as step-bunching.[27] Reference 28 provides a recent review of MOCVD growth of c-plane AlGaN for deep-ultraviolet LEDs. We also note that AlN and high Al-content AlGaN have also been grown by MOCVD on m-plane AlN,[29,30] and other substrates[31] with applications in UV emitters.[32] Bryan *et al*. discussed the effects of surface kinetics on the composition distribution of c-plane AlGaN grown by MOCVD.[27] They found that substrate surface morphology, in particular, step-structure determined by miscut, has a strong effect on AlGaN composition inhomogeneities. They proposed a model that employs different surface residence times for Ga and Al to explain the formation of composition columns tilted with respect to the growth direction. Step bunching was associated with Al-content variation. Ga-rich alloys are formed on short terraces, while Al-rich alloys are formed on long terraces. Their model may explain the composition non-uniformities of m-plane AlGaN as well. In our case, we speculate that AlGaN growth on m-plane GaN undergoes a step-bunching transition with increasing film thickness with the steps parallel to the c-axis. Initially, the GaN surface has relatively long terraces in the a-direction that result in growth of high-Al layers (substrate miscut towards the -c direction). However, the surface is unstable to step-bunching in the a-direction. The m-type nanofacets on the side of the stripes visible in Figs. 1(a) and 3(a) are likely the result of this step-bunching instability. Once the step-bunches are formed, the Ga incorporation increases and the Al composition drops correspondingly to a lower value in the flat-top islands.

CONCLUSIONS

In conclusion, we examined the growth of AlGaN on m-plane GaN by plasma-enhanced MBE under Ga-rich conditions and observed an unprecedented kinetic instability of high Al-composition AlGaN. We found that above a critical Al flux the AlGaN growth rate is drastically suppressed to a level close to that of AlN, and the growth mode can be referred to as Al-limited growth in Ga-rich conditions. The defect structure characteristic to this regime was studied with STEM-EDX. Under these growth conditions, m-plane AlGaN develops a unique nanostructure characterized by Al-rich thin planar films and flat-top stripes bordered by m-type nano-facets. Our experimental results support a model in which Al-N dimers promote Ga-N dimer detachment from c-type edges on the surface. The composition variation in the nanostructures can be explained by step-bunching in the direction of the a-axis, but more theoretical work is needed to substantiate our models. Experimentally, we believe that careful control of the substrate miscut in the a- and c-direction can be used to promote m-plane growth of uniform AlGaN layers.

ACKNOWLEDGMENTS

We acknowledge support from the U.S. National Science Foundation. M.S.-HD was supported, in part, by NSF Award DMR-1610893. T.N. and O.M. acknowledge partial support from NSF Grant No. ECCS-1253720. Part of the TEM/STEM work was supported by the U.S. National Science Foundation Grant No. DMR-1565822.

[1]M. Beeler, E. Trichas, and E. Monroy, Semicond. Sci. Technol. **28**, 074022 (2013).
[2]C. Edmunds, J. Shao, M. Shirazi-HD, M. J. Manfra, and O. Malis, Appl. Phys. Lett. **105**, 021109 (2014).
[3]O. Malis, C. Edmunds, D. Li, J. Shao, G. Gardner, W. Li, P. Fay, and M. J. Manfra, Proc. SPIE **9002**, 90021D (2014).
[4]T. Kotani, M. Arita, and Y. Arakawa, Appl. Phys. Lett. **105**, 261108 (2014).
[5]T. Kotani, M. Arita, and Y. Arakawa, Appl. Phys. Lett. **107**, 112107 (2015).
[6]T. Kotani, M. Arita, K. Hoshino, and Y. Arakawa, Appl. Phys. Lett. **108**, 052102 (2016).
[7]C. B. Lim, M. Beeler, A. Ajay, J. Lahnemann, E. Bellet-Amalric, C. Bougerol, and E. Monroy, J. Appl. Phys. **118**, 014309 (2015).
[8]C. B. Lim, A. Ajay, C. Bougerol, B. Hass, J. Schormann, M. Beeler, J. Lahnemann, M. Eickhoff, and E. Monroy, Nanotechnology **26**, 435201 (2015).
[9]C. B. Lim, A. Ajay, C. Bougerol, J. Lahnemann, F. Donatini, J. Schormann, E. Bellet-Amalric, D. A. Browne, M. Jimenez-Rodriguez, and E. Monroy, Nanotechnology **27**, 145201 (2016).
[10]C. B. Lim, M. Beeler, A. Ajay, J. Lahnemann, E. Bellet-Amalric, C. Bougerol, J. Schormann, M. Eickhoff, and E. Monroy, Jpn. J. Appl. Phys., Part 1 **55**, 05FG05 (2016).
[11]C. B. Lim, A. Ajay, C. Bougerol, E. Bellet-Amalric, J. Schormann, M. Beeler, and E. Monroy, Phys. Status Solidi A **214**, 1600849 (2017).
[12]A. Pesach, E. Gross, C.-Y. Huang, Y.-D. Lin, A. Vardi, S. E. Schacham, S. Nakamura, and G. Bahir, Appl. Phys. Lett. **103**, 022110 (2013).
[13]M. Sawicka, H. Turski, M. Siekacz, J. Smalc-Koziorowska, M. Krysko, I. Dziecielewski, I. Grzegory, and C. Skierbiszewski, Phys. Rev. B **83**, 245434 (2011).
[14]M. Sawicka, C. Cheze, H. Turski, J. Smalc-Koziorowska, M. Krysko, S. Kret, T. Remmele, M. Albrecht, G. Cywinski, I. Grzegory, and C. Skierbiszewski, J. Cryst. Growth **377**, 184 (2013).
[15]J. Smalc-Koziorowska, M. Sawicka, T. Remmele, C. Skierbiszewski, I. Grzegory, and M. Albrecht, Appl. Phys. Lett. **99**, 061901 (2011).
[16]M. Sawicka, A. Feduniewicz-Żmuda, H. Turski, M. Siekacz, S. Grzanka, M. Kryśko, I. Dzięcielewski, I. Grzegory, and C. Skierbiszewski, J. Vac. Sci. Technol. B **29**, 03C135 (2011).
[17]J. Shao, L. Tang, C. Edmunds, D. Zakharov, O. Malis, and M. J. Manfra, Appl. Phys. Lett. **103**, 232103 (2013).
[18]J. Shao, L. Tang, C. Edmunds, G. Gardner, O. Malis, and M. J. Manfra, J. Appl. Phys. **114**, 023508 (2013).
[19]H. Morkoç, *Handbook of Nitride Semiconductors and Devices* (Wiley VCH Verlag GmbH & Co. KGaA, Weinheim, 2008).
[20]L. Lymperakis and J. Neugebauer, Phys Rev. B. **79**, 241308(R) (2009).
[21]V. Jindal and F. Shahedipour-Sandvik, J. Appl. Phys. **105**, 084902 (2009).
[22]E. Iliopoulos, K. F. Ludwig, Jr., T. D. Moustakas, P. Komninou, T. Karakostas, G. Nouet, and S. N. G. Chu, Mater. Sci. Eng., B **87**, 227 (2001).
[23]E. Iliopoulos and T. D. Moustakas, Appl. Phys. Lett. **81**, 295 (2002).
[24]M. Horita, T. Kimoto, and J. Suda, Appl. Phys. Express **2**, 091003 (2009).
[25]C. B. Lim, A. Ajay, and E. Monroy, Appl. Phys. Lett. **111**, 022101 (2017).
[26]Z. Liu, R.-Z. Wang, and P. Zapol, Phys. Chem. Chem. Phys. **18**, 29239 (2016).
[27]I. Bryan, Z. Bryan, S. Mita, A. Rice, L. Hussey, C. Shelton, J. Tweedie, J.-P. Maria, R. Collazo, and Z. Sitar, J. Cryst. Growth **451**, 65 (2016).
[28]K. Ding, V. Avrutin, U. Ozgur, and H. Morkoc, Crystals **7**, 300 (2017).
[29]I. Bryan, Z. Bryan, M. Bobea, L. Hussey, R. Kirste, R. Collazo, and Z. Sitar, J. Appl. Phys. **116**, 133157 (2014).
[30]J. Nishinaka, Y. Taniyasu, T. Akasaka, and K. Kumakura, Phys. Status Solidi **254**, 1600545 (2017).
[31]J. Suda, M. Horita, R. Armitage, and T. Kimoto, J. Cryst. Growth **301–302**, 410 (2007).
[32]R. G. Banal, Y. Taniyasu, and H. Yamamoto, Appl. Phys. Lett. **105**, 053104 (2014).